ADVANCES IN ATMOSPHERIC SCIENCES, VOL. 25, NO. 4, 2008, 619–631

An Updated Coupled Model for Land-Atmosphere Interaction. Part I: Simulations of Physical Processes

ZENG Hongling[1,2,3] (曾红玲), WANG Zaizhi[2] (王在志), JI Jinjun[4] (季劲钧), and WU Guoxiong[*1] (吴国雄)

[1] *State Key Laboratory of Numerical Modeling for Atmospheric Sciences and Geophysical Fluid Dynamics, Institute of Atmospheric Physics, Chinese Academy of Sciences, Beijing* 100029

[2] *National Climate Center, Beijing* 100081

[3] *Graduate University of Chinese Academy of Sciences, Beijing* 100049

[4] *START Regional Research Center for Temperate East Asia, Institute of Atmospheric Physics, Chinese Academy of Sciences, Beijing* 100029

(Received 16 May 2007; revised 10 December 2007)

ABSTRACT

A new two-way land-atmosphere interaction model (R42_AVIM) is fulfilled by coupling the spectral atmospheric model (SAMIL_R42L9) developed at the State Key Laboratory of Numerical Modeling for Atmospheric Sciences and Geophysical Fluid Dynamics, Institute of Atmospheric Physics, Chinese Academy of Sciences (LASG/IAP/CAS) with the land surface model, Atmosphere-Vegetation-Interaction-Model (AVIM). In this coupled model, physical and biological components of AVIM are both included. Climate base state and land surface physical fluxes simulated by R42_AVIM are analyzed and compared with the results of R42_SSIB [which is coupled by SAMIL_R42L9 and Simplified Simple Biosphere (SSIB) models]. The results show the performance of the new model is closer to the observations. It can basically guarantee that the land surface energy budget is balanced, and can simulate June–July–August (JJA) and December-January-February (DJF) land surface air temperature, sensible heat flux, latent heat flux, precipitation, sea level pressure and other variables reasonably well. Compared with R42_SSIB, there are obvious improvements in the JJA simulations of surface air temperature and surface fluxes. Thus, this land-atmosphere coupled model will offer a good experiment platform for land-atmosphere interaction research.

Key words: SAMIL-R42L9, R42_AVIM, R42_SSIB, land-atmosphere coupling

DOI: 10.1007/s00376-008-0619-y

1. Introduction

Land surface processes are among the most important components in a climate system. The state of land surface determines the energy and water balance at the interface of land and atmosphere to a great extent. By exchanging water, heat, energy and material interactions can occur with the atmosphere. Different regional climate and atmospheric circulations are formed mainly due to various land surface types. Vegetation is an important characteristic of a land surface. The physiological and morphologic characteristics of vegetation have important influences on land surface processes, and the interaction between vegetation and atmosphere is an important issue concerning the study of climate change. As is well known, geographical distribution and productivity of vegetation are determined by climate factors such as precipitation, temperature, radiation, atmospheric CO_2 concentration, etc. At the same time vegetation can also have feedbacks on the climate. Vegetation can change climate by exerting an influence on the exchanging of energy, mass and momentum. Biogeochemistry processes can also be changed by the exchange of CO_2 through vegetation (Pielke et al., 1998; Bonan, 2002; Kaufmann et al., 2003). However, since earlier research work on

*Corresponding author: WU Guoxiong, gxwu@lasg.iap.ac.cn

land parameter sensitivities (Charney, 1975; Charney et al., 1977; Shukla and Mintz, 1982; Yeh et al., 1984; Sud and Smith, 1985), most work about vegetation-atmosphere interaction focuses on one-sided research. That is, using prescribed change of land surface parameters to study the response of climate, and ignoring the interaction and feedbacks between them. In the climate system models, assigned vegetation classification, leaf area index (LAI) and vegetation fraction are generally used as well. In recent study, some models take the two-way coupling of the vegetation and atmosphere into account. For instance, Foley et al. (1998) coupled the vegetation model IBIS (Version 1.0) with the general circulation model GENESIS (Version 2.0), and simulated the preliminary position of forest and grassland; Cox (2001) added a global dynamic vegetation model TRIFFID into the Hadley atmosphere-ocean coupling model HadCM3; Lu et al. (2001) coupled the regional climate model RAMS with the ecosystem model CENTUARY, and studied the biological processes in central U.S.A. on a weekly time scale; Tsvetsinskaya et al. (2001) incorporated the crop growing model CERES-Maize to BATS, and estimated the effect of crop growing on surface flux exchanges; Snyder et al. (2004) added global dynamical vegetation model IBISI into the general circulation model CCM3, and studied the influence of vegetation change on regional precipitation; Dan et al. (2005) coupled AVIM into the GOALS AGCM_R15L9, and found that the two-way land-atmosphere coupled model can basically simulate the distribution of the global climate basic state and biomass on land. All the above work related to two-way coupling between land and atmosphere is still preliminary and the GCM resolution is relatively low. However, the land/vegetation distribution is very complex, and these models can't meet the requirement of rationally describing the land status. Therefore, it is essential to develop or integrate a relatively higher resolution two-way land-atmosphere coupled model.

In this study, by coupling a higher resolution GCM SAMIL_R42L9 with AVIM, a new two-way vegetation-atmosphere interaction coupled model is fulfilled. The simulated climate base states and the surface physical fluxes obtained from integrating the R42_AVIM are then compared with the results simulated by the model R42_SSIB. The simulations of the biological processes will be discussed in a parallel paper. This study is organized as follows: section 2 introduces the models used in this work; section 3 describes the coupling design and the observational data; section 4 evaluates the model simulation results. In the last part of the article, the conclusions and discussions are given.

2. Model descriptions

2.1 *SAMIL-R42L9*

SAMIL_R42L9 is a nine-level spectral atmospheric general circulation model developed at LASG/IAP. It is rhomboidally truncated at zonal wave number 42, approximately 2.8125° lon×1.66° lat. The unique dynamic framework, by subtracting "a standard atmosphere" from the set of governing equations, was introduced to the model to reduce errors (Zeng, 1963). A new radiation scheme by Edwards and Slingo (1996) and a cloud fraction diagnosis scheme which depends on relative humidity and vertical velocity (Slingo, 1987), have been gradually introduced into SAMIL_R42L9. In addition, the model also considers other sub-grid physical processes, such as the convective parameterization scheme (Manabe et al., 1965). The model time step is set to 15 minutes, adopting a semi-implicit scheme. Radiative fluxes are updated every six hours. Forced by 30-year (1971–2000) averaged climatological monthly mean sea surface temperature and sea-ice fraction concentration, the model can capture the main characteristics of the global and regional climate basic state (Wu et al., 2003). A detailed introduction of this model can be found in Zhang et al. (2000) and Wang et al. (2004).

2.2 *AVIM (atmosphere-vegetation interaction model)*

AVIM was developed by incorporating a plant physiological process to the Land Surface Process Model (LPM) (Ji and Hu, 1989; Ji, 1995). It includes both physical processes and physiological processes at the land surface. The former relates to energy and water cycles between soil, vegetation and air, whereas the latter deals with carbon exchange between them, including photosynthesis, respiration, dry matter allocation and phenological processes of plants. LAI is the key parameter to link the above physical and physiological processes. That is, LAI varies with vegetation growth and thus results in the change of physical parameters such as albedo, zero displacement height and stoma resistance etc. All these changes will in turn alter the energy and water balance on the surface and consequently, the vegetation growth is affected. This is a dynamic and interactive process. This model has been tested in different terrestrial ecosystems and proved to have excellent performance (Ji, 1995; Ji and Yu, 1999; Lu, 1999; Li and Ji, 2001; Lu and Ji, 2002a,b; Lu and Ji, 2006).

3. Coupling design and observational data used

The exchange of heat, momentum and water vapor between the atmosphere and the land are mainly manifested in the vertical diffusion term of the atmospheric motion equations. The flux equations are as follows:

$$(\boldsymbol{F}_{\rm v}, F_{\rm v}^{T}, F_{\rm v}^{M}) = \frac{g}{p^*}\frac{\partial}{\partial\sigma}\{\boldsymbol{\tau}, H/c_p, E\}\ , \tag{1}$$

$$\boldsymbol{\tau} = \rho C_{\rm D}|\boldsymbol{V}_{\rm a}|\boldsymbol{V}_{\rm a}\ , \tag{2}$$

$$H = \rho c_p(\theta_{\rm ac} - \theta_{\rm a})/r_{\rm a}\ , \tag{3}$$

$$E = \rho(q_{\rm ac} - q_{\rm a})/r_{\rm a}\ , \tag{4}$$

in which, subscript "v" denotes the vertical direction, thus $\boldsymbol{F}_{\rm v}, F_{\rm v}^{T}, F_{\rm v}^{M}$, are vertical momentum, heat and water vapor fluxes respectively. $\boldsymbol{\tau}, H, E$ are transfers of momentum, heat and water vapor fluxes between air and land. $\boldsymbol{V}_{\rm a}, \theta_{\rm a}$, and $q_{\rm a}$ are air velocity, potential temperature and specific humidity at the bottom layer of GCM. ρ is air density. $\theta_{\rm ac}$ and $q_{\rm ac}$ are potential temperature and specific humidity within the canopy, respectively. $C_{\rm D}$ and c_p are drag coefficient and specific heat at constant pressure. $r_{\rm a}$ is aerodynamical resistance at the surface layer.

In this study, we coupled SAMIL-R42L9 and AVIM grid by grid. LAI is not prescribed as it is by many other models, but is dynamically computed. The physical and biological components of AVIM are both included and connected in the land-atmosphere coupled model R42_AVIM. Using the climatological mean SST, we run the model for 15 years and take the mean of the last 10 years as climate basic state. To examine different fields simulated by the R42_AVIM, we use the following observational data: (1) 1979–1998 global reanalysis of the National Centers for Environmental Prediction (NCEP) (Kalnay et al., 1996), including surface air temperature, sea level pressure, wind, surface sensible, latent heat fluxes etc. (2) 1979–1998 global reanalysis of the European Centre for Medium-Range Weather Forecasts (ECMWF) (Simmons and Gibson, 2000; Uppala et al., 2005), including surface sensible, latent heat fluxes etc. (3) 1979–1998 global $2.5^\circ \times 2.5^\circ$ gridded data of monthly precipitation from Xie and Arkin (1996). In addition, the climate basic state and surface physical fluxes of R42_AVIM are analyzed and compared with the simulation results of R42_SSIB. Here, R42_SSIB is coupled by SAMIL_R42L9 and the Simplified Simple Biosphere (SSIB) model. Similarly, we also run it for 15 years and analyze the mean of the last 10 years.

4. Results

4.1 *Energy budget on air-land interface*

Energy budget on land surface can be expressed as:

$$S\downarrow(1-\alpha)+L\downarrow-L\uparrow-{\rm SH}-{\rm LH}+G+F=0 \tag{5}$$

In the above formula, $S\downarrow, L\downarrow$ and $L\uparrow$ are the net downward short wave radiation, surface absorbed and emitted long wave radiation. α is surface albedo. SH and LH are surface sensible and latent heat fluxes. G is downward soil heat flux and F is the chemical energy produced by vegetation photosynthesis and respiration. According to the work of Sellers (1992), G and F are less than 1% of the total surface energy, so they are usually ignored in climate simulation study.

Simulation of R42_AVIM shows that the annual mean energy budget on global land surface is 0.167 W m^{-2}, which is relatively small and to some extent tends to be balanced. This can assure the rationality of the simulated results and provide an important guarantee for next generation of ocean-land-atmosphere coupled climate system models.

4.2 *Surface air temperature*

Figure 1 shows the global distribution of DJF mean surface air temperature derived from R42_AVIM and NCEP reanalysis. In addition, the differences between R42_AVIM, R42_SSIB and NCEP are also presented. Compared with NCEP reanalysis (Fig. 1b), R42_AVIM does well in reproducing the basic patterns of observed surface air temperature in DJF (Fig. 1a). However, biases still exist. From Fig. 1c, in Europe, Northeast Canada and on the Tibetan plateau, the simulated surface air temperature is warmer than NCEP reanalysis with a bias above 4°C. There is a cold bias of 2°C–4°C in northern South America. For R42_SSIB (Fig. 1d), similar to R42_AVIM, there exist 2°C–4°C warm biases between simulation and NCEP reanalysis in Europe, Northeast Canada and on the Tibetan plateau. Differently, there are a 4°C–6°C cold bias to the northeast of Baikal, 8°C cold bias to the north of Russia and 2°C–4°C cold bias in West Asia and Mexico. In Southern Hemisphere, the R42_SSIB simulation on land is widely warmer, especially in the south of Brazil with a range of 8°C. We can clearly see that, compared with R42_SSIB, there are obvious improvements in the R42_AVIM simulation of surface air temperature in northeastern Baikal, north of Russia, Mexico and West Asia, but there still have a warm bias center of 8°C on the Tibetan plateau and a cold bias center of 2°C–4°C in northern South America.

Figure 2 is the same as Fig. 1, but for June–July–August (JJA). In boreal summer, surface air temperature rises rapidly, showing a dramatic seasonal change.

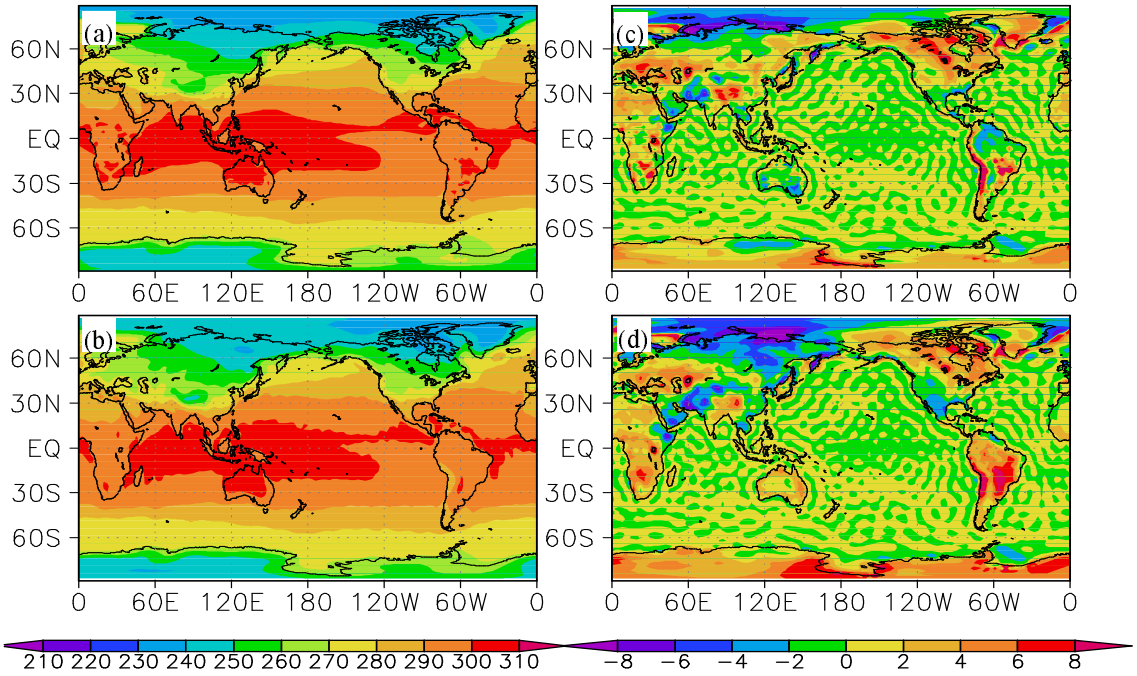

Fig. 1. The DJF mean surface temperature derived from (a) R42_AVIM, (b) NCEP reanalysis, and the difference between (c) R42_AVIM and NCEP reanalysis, (d) R42_SSIB and NCEP reanalysis. Units: K.

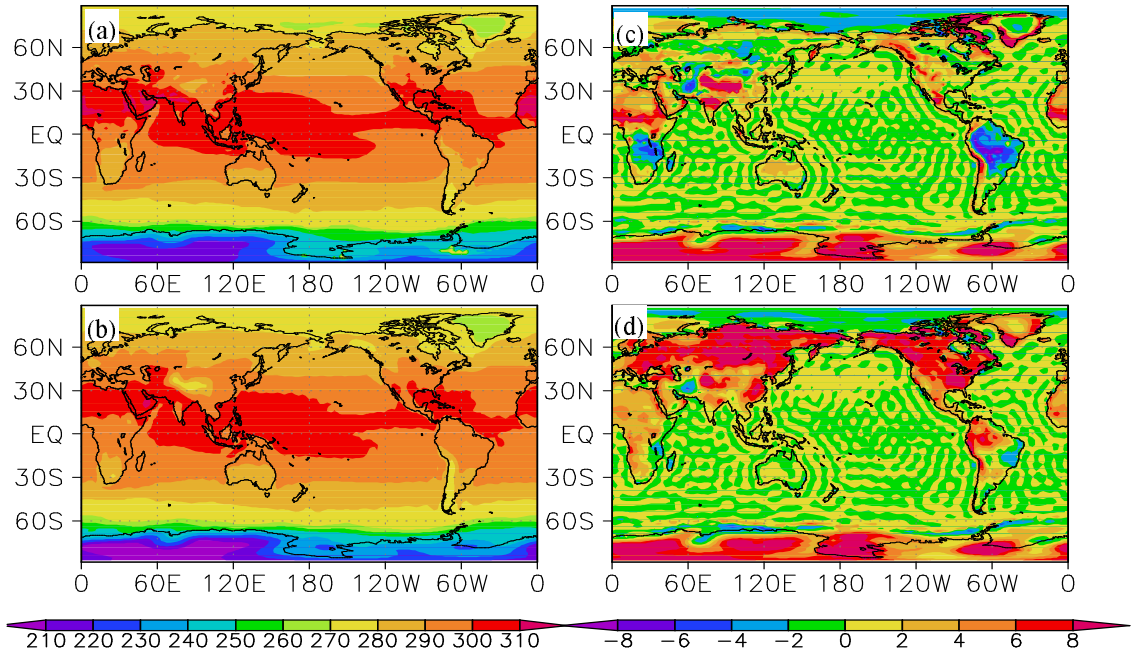

Fig. 2. The JJA mean surface temperature derived from (a) R42_AVIM, (b) NCEP reanalysis, and the difference between (c) R42_AVIM and NCEP reanalysis, (d) R42_SSIB and NCEP reanalysis. Units: K.

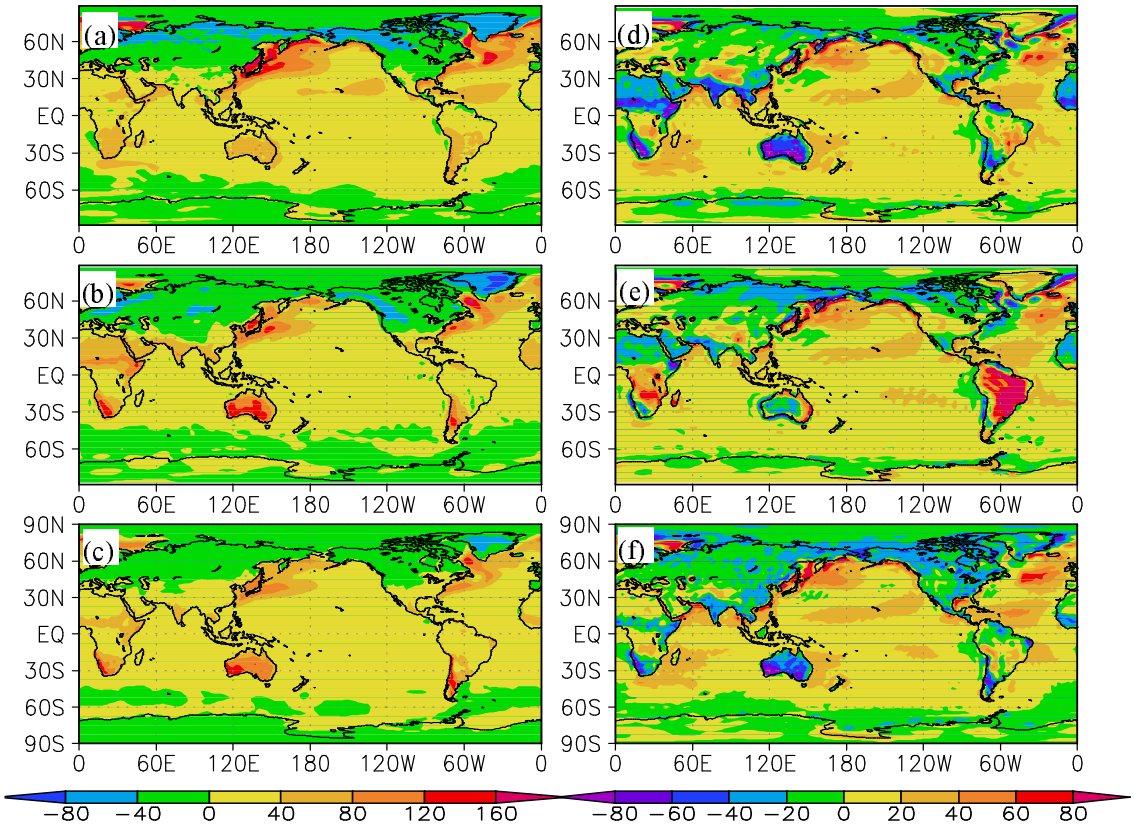

Fig. 3. The DJF mean surface sensible heat flux derived from (a) R42_AVIM, (b) NCEP reanalysis, (c) ECMWF reanalysis and the difference between (d) R42_AVIM and NCEP reanalysis, (e) R42_SSIB and NCEP reanalysis, (f) R42_AVIM and ECMWF reanalysis. Units: W m^{-2}.

JJA surface air temperature derived from R42_AVIM (Fig. 2a) is close to NCEP reanalysis (Fig. 2b). However, there exists a 2°C–4°C colder zone along 60°N across the Eurasian continent. In South Africa, West Asia and northern South America, there are also cold biases with a range of 4°C–6°C. Over the Tibetan plateau, like in DJF, there still exists a warm bias of 8°C (Fig. 2c). This is probably attributed to the terrain scheme and needs to be corrected. In addition, in arid or semi-arid regions such as the Sahara, India and Alaska, there are warm biases as well. This shows that we should improve the surface parameters on those areas. For R42_SSIB (Fig. 2d), there are obviously warm biases above 6°C in the broad regions of Asia, Europe and North America, and even close to 10°C in some regions near Lake Baikal. The simulation in the Southern Hemisphere is better than that in the Northern Hemisphere. The simulated surface air temperature is close to NCEP reanalysis in Australia. However, the surface air temperature over most parts of Africa and South America is warmer than NCEP reanalysis and there is a cold bias of 2°C–4°C in East Brazil. R42_AVIM has greatly improved the simulation of JJA surface air temperature, especially in the broad areas of Asia, Europe and North America. As well known, the characteristics of vegetation and soil can determine the surface energy budget and temperature. In AVIM, vegetation physiological process is considered and the interactions and feedbacks between vegetation and atmosphere are realized. Due to improvements in the surface process parameterizations, the simulation of surface air temperature is also more reasonable. On the other hand, the soil in AVIM is subdivided into 10 uneven layers and soil wetness can be simulated more precisely. This also offers help for the simulation of surface air temperature.

4.3 *Surface sensible heat flux*

Figure 3 shows the global distribution of DJF mean surface sensible heat flux, including R42_AVIM simulation results, NCEP reanalysis, ECMWF reanalysis and the differences between R42_AVIM, R42_SSIB and NCEP reanalysis, as well as the difference between R42_AVIM and ECMWF reanalysis. In winter, the cold air from continents blows to the west coasts of oceans continuously, which leads to the large differ-

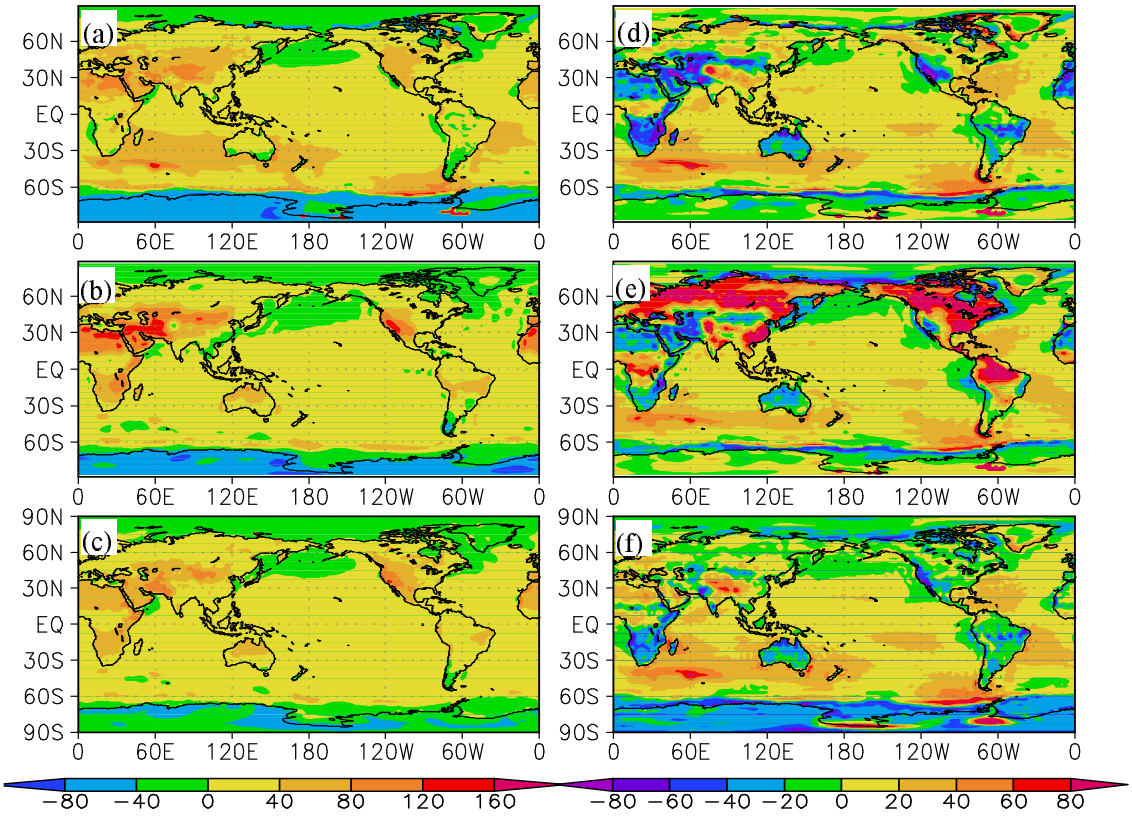

Fig. 4. The JJA mean surface sensible heat flux derived from (a) R42_AVIM, (b) NCEP reanalysis, (c) ECMWF reanalysis and the difference between (d) R42_AVIM and NCEP reanalysis, (e) R42_SSIB and NCEP reanalysis, (f) R42_AVIM and ECMWF reanalysis. Units: W m^{-2}.

ence of temperature between land and sea. So the maximum sensible heat flux is distributed in the northwest of Pacific and Atlantic. It can also be clearly seen that on the continents, the sensible heat flux is negative north of 30°N, transferring heat from the atmosphere to the land. However, the sensible heat flux is positive south of 30°N, and land surface releases heat to the atmosphere (Figs. 3a–c). Compared with NCEP and ECMWF reanalysis, R42_AVIM can basically simulate the distribution of sensible heat flux, but there are biases too. Compared to NCEP reanalysis, R42_AVIM has about 60 W m^{-2} less sensible heat flux in Australia and tropical Africa. However, the simulation is larger in southeastern South America and on the Tibetan plateau (Fig. 3d). For R42_SSIB, the largest difference is situated in South America, having a bias of more than 100 W m^{-2}, which is consistent with the warm bias of surface temperature over there. In addition, the sensible heat flux is larger in South Africa and on the Tibetan plateau while less in northeastern Baikal, which is also related to the simulated surface air temperature (Fig. 3e). ECMWF reanalysis is similar to NCEP reanalysis, but a little larger in most areas of the Northern Hemisphere. However, in tropical Africa and over Indian peninsula, NCEP reanalysis is larger. So, in tropical Africa, over Indian peninsula and on the Tibetan Plateau, DJF sensible heat flux from R42_AVIM is closer to ECMWF reanalysis (Fig. 3f). From above, it shows that R42_AVIM has improved the simulation in South America and South Africa, but still has a low bias in Austria and tropical Africa.

Figure 4 is the same as Fig. 3, but for JJA. In boreal summer, with the rise of temperature, the surface sensible heat flux increases rapidly too. Over almost the entire mainland the sensible heat flux is positive. However, over the North Pacific and Atlantic, it is negative (Figs. 4a–c). Compared with the NCEP reanalysis, the simulated sensible heat flux by R42_AVIM is less to a certain extent in the Sahara, west Asia, Australia, South Africa, north of the Tibetan plateau, the west coast of America and South America (Fig. 4d). However, it is closer to ECMWF reanalysis in above areas (Fig. 4f). For R42_SSIB simulated sensible heat flux, it is obviously higher than NCEP reanalysis on nearly all the continents with biases above 100 W m^{-2} in some local regions. This is consistent with the obviously warm bias of the simulated surface air temper-

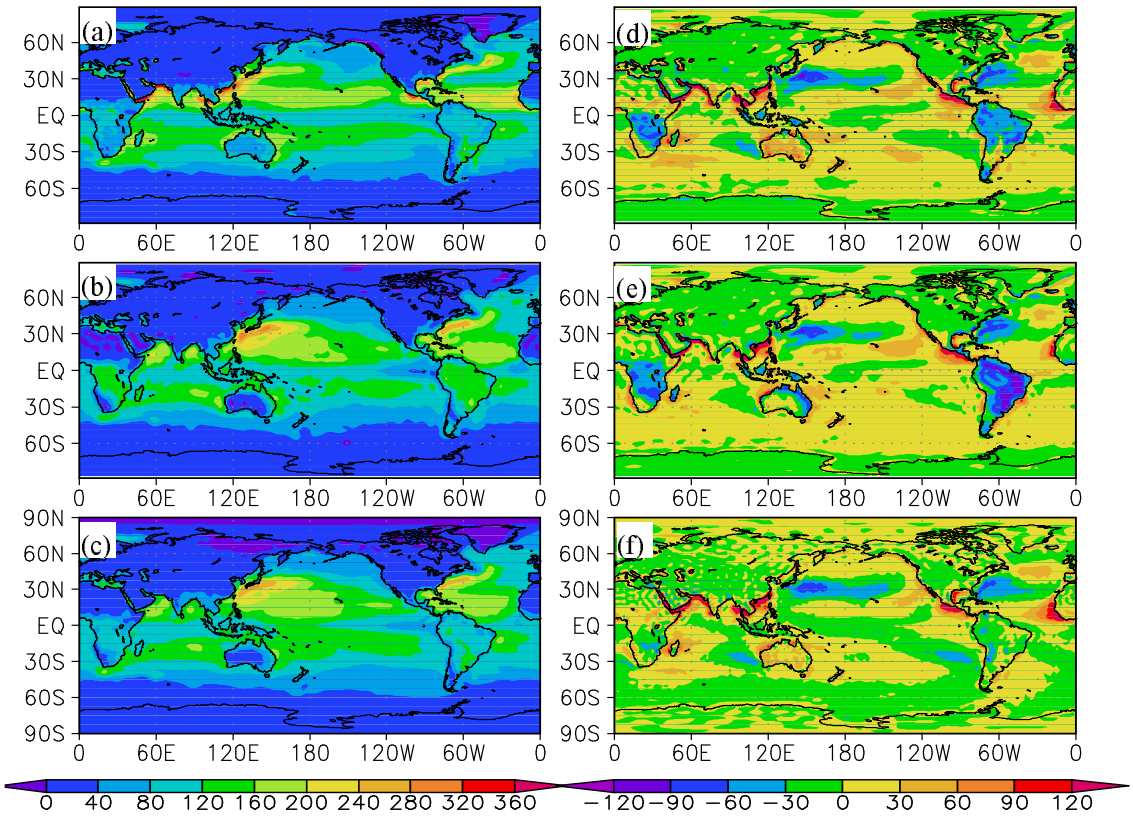

Fig. 5. The DJF mean surface latent heat flux derived from (a) R42_AVIM, (b) NCEP reanalysis, (c) ECMWF reanalysis and the difference between (d) R42_AVIM and NCEP reanalysis, (e) R42_SSIB and NCEP reanalysis, (f) R42_AVIM and ECMWF reanalysis. Units: W m^{-2}.

ature (Figs. 4e, 2d). R42_AVIM has greatly improved the simulation of JJA sensible heat flux, indicating that vegetation has a similar regulation on the simulation of surface heat flux.

4.4 *Surface latent heat flux*

Similar to Fig. 3, Fig. 5 displays the global distribution of DJF mean surface latent heat flux. In winter, maximum surface latent heat flux is mainly distributed over the seas, especially the subtropical oceans of both hemispheres. In the extratropical regions of the northern hemisphere, the temperature is low. Vegetation nearly stops growing, and the surface latent heat flux is close to zero. The simulation derived from R42_AVIM and R42_SSIB are both close to the NCEP and ECMWF reanalysis in the northern hemisphere (Figs. 5a–f). In the southern hemisphere, compared with NCEP reanalysis, both models have a low bias in South Africa and northern South America. However, the simulation of R42_SSIB is lower than that of R42_AVIM in South America. In Australia, the simulation of R42_SSIB is closer to NCEP reanalysis (Figs. 5d, e). Surface latent heat flux from ECMWF reanalysis is less than NCEP reanalysis in South Africa and northern South America, so R42_AVIM compares quite well to it (Figs. 5c, f).

Figure 6 is the surface latent heat flux in JJA. In boreal summer, with the increasing of air temperature and vegetation in its growing season, surface latent heat flux rises greatly and has a clearly seasonal change (Figs. 6a–c). The distribution of surface latent heat flux simulated by R42_AVIM is basically consistent with the NCEP and ECMWF reanalysis. However, compared with NCEP reanalysis, the simulated value is about 30 W m^{-2} lower than NCEP reanalysis in general (Fig. 6d). ECMWF reanalysis is less than NCEP reanalysis in most land areas, which leads to the R42_AVIM simulation being closer to it (Fig. 6f) For R42_SSIB (Fig. 6e), the simulated surface latent heat flux has a low bias of about 80 W m^{-2} on nearly all continents except for Australia, some parts of the Sahara and the area surrounding the Tibetan plateau. In southeastern North America, the bias is even above 100 W m^{-2}. In AVIM, vegetation growth process is considered and vegetation is interactive with climate. This is helpful for the simulation of vegetation evaporation and transpiration, thus in turn improves the simulation of surface latent heat flux in R42_AVIM.

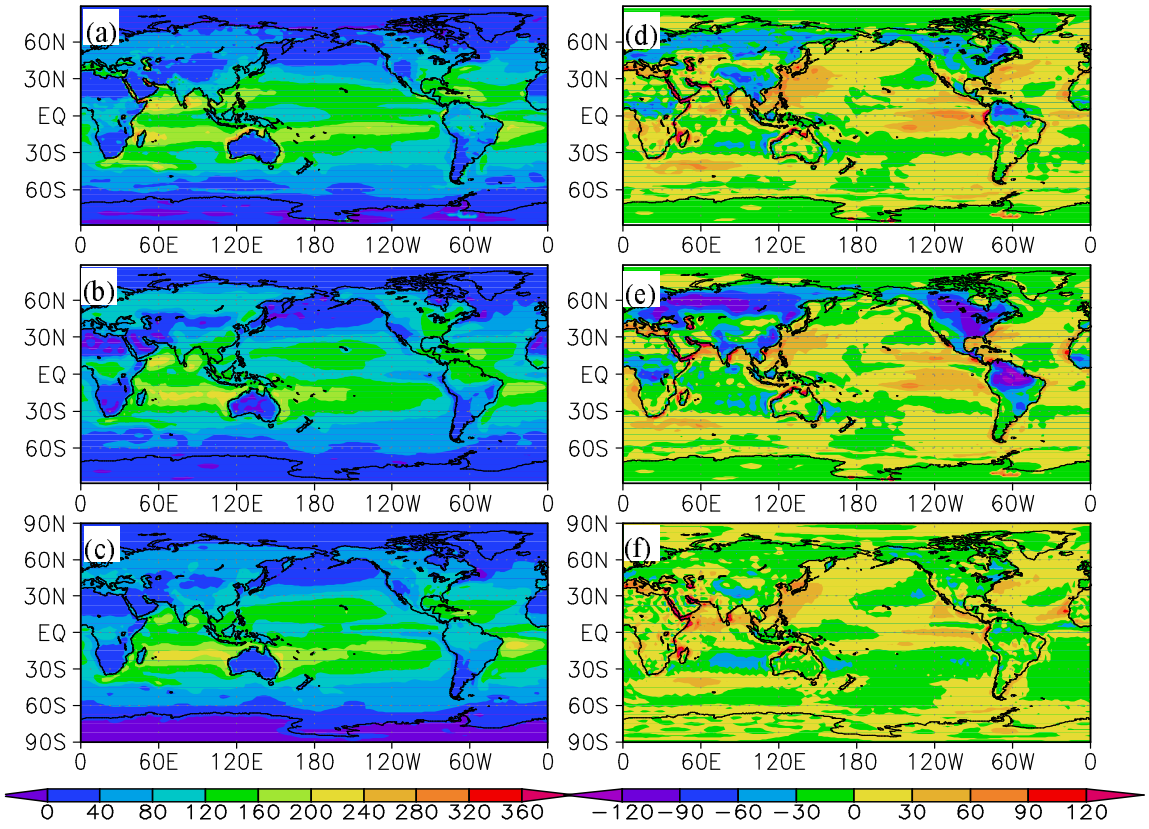

Fig. 6. The JJA mean surface latent heat flux derived from (a) R42_AVIM, (b) NCEP reanalysis, (c) ECMWF reanalysis and the difference between (d) R42_AVIM and NCEP reanalysis, (e) R42_SSIB and NCEP reanalysis, (f) R42_AVIM and ECMWF reanalysis. Units: W m^{-2}.

Table 1. DJF and JJA global land averaged surface air temperature (TS), surface sensible heat flux (HFSS) and surface latent heat flux (HFLS) from NCEP reanalysis, R42_AVIM and R42_SSIB.

	NCEP DJF (JJA)	R42_AVIM DJF (JJA)	R42_SSIB DJF (JJA)
TS (K)	276.573 (286.764)	277.776 (288.677)	277.826 (290.93)
HFSS (W m^{-2})	16.1647 (35.905)	3.66941 (27.1635)	21.7936 (62.9815)
HFLS (W m^{-2})	44.0126 (61.6885)	31.313 (46.9006)	22.1272 (24.7785)

In order to give a direct impression on model simulation, global land averaged results are given too. Table 1 is the DJF and JJA global land averaged surface air temperature, surface sensible heat flux and surface latent heat flux from NCEP reanalysis, R42_AVIM and R42_SSIB. In DJF and JJA, surface air temperature from R42_AVIM and R42_SSIB are both warmer than NCEP reanalysis. In DJF, the difference between R42_SSIB and NCEP reanalysis is 1.253°C and is 1.203°C for R42_AVIM. In JJA, the two values are 4.166°C and 1.913°C respectively. It shows that R42_AVIM is closer to NCEP reanalysis, especially in JJA. For surface sensible heat flux, in DJF and JJA, R42_AVIM is less while R42_SSIB is more than the NCEP reanalysis. In JJA, R42_SSIB is 27.08 W m^{-2} more than the NCEP reanalysis. R42_AVIM has greatly corrected the excessive surface sensible heat flux simulated by R42_SSIB, although it is 8.74 W m^{-2} less than NCEP reanalysis. The two models both give less surface latent heat flux. In DJF and JJA, the differences between R42_AVIM and NCEP reanalysis are 12.7 W m^{-2} and 14.79 W m^{-2} respectively, while they are 21.9 W m^{-2} and 36.9 W m^{-2} for R42_SSIB. So, R42_AVIM has improved the simulation of surface latent heat flux to a certain extent.

4.5 *Precipitation*

4.5.1 *Zonally land averaged features*

The zonal mean DJF and JJA land precipitation rates derived from R42_AVIM, R42_SSIB and Xie-

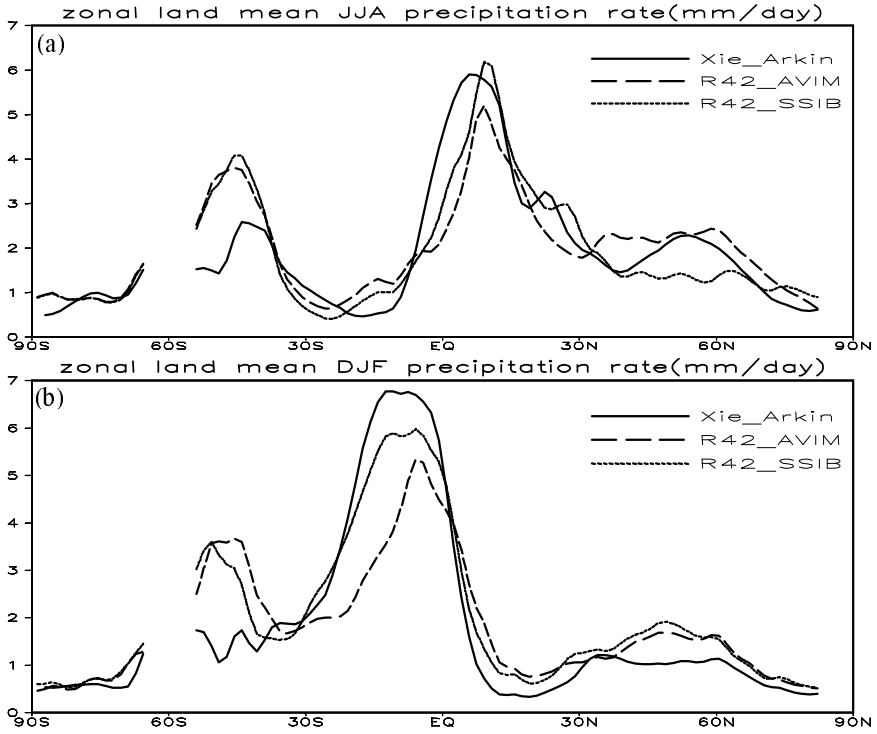

Fig. 7. The (a) DJF, (b) JJA zonal mean precipitation rate derived from R42_AVIM and XIE-ARKIN.Units: mm d^{-1}.

Arkin are shown in Fig. 7. In general, the distribution from R42_AVIM and R42_SSIB are consistent with Xie_Arkin data. The maximum precipitation is centralized in the tropics with the second maximum over the middle latitudes and the minimum in the subtropical regions in both seasons. However, some biases still exist between the simulation and Xie_Arkin data. In DJF, the tropical precipitation maximum from Xie_Arkin is larger than the two simulations. In addition, the precipitation from R42_SSIB is more than that from R42_AVIM between 30°S and the equator. However, the two simulations have more precipitation over the land of other latitudes, especially in the Southern Hemisphere (Fig. 7a). In boreal summer, the simulated maximum precipitation from R42_SSIB is larger than observation while R42_AVIM is less in the tropics. In 0°–10°N, the two simulations are less than the observation. However, they are both larger in 30°–60°S. In 40°–70°N, R42_SSIB has much less precipitation than Xie_Arkin. (Fig. 7b). These simulation differences may be attributed to the bias of simulated specific humidity (not shown).

4.5.2 *Global distribution*

Figure 8 shows the global geographical distributions of the DJF and JJA precipitation rate derived from R42_AVIM, Xie-Arkin data and their difference. In winter, the large rainfall simulated by R42_AVIM is located over the western parts of the South Pacific and South Atlantic, near the equator, South Africa, Southeast Asia and the South American continent. The secondary maximum of precipitation is situated over the mid-latitudes where fronts and their associated disturbances usually predominate, while the low rainfall is situated over the eastern parts of oceans and in high latitudes in both hemispheres. All the above simulation results are consistent with the observational data (Figs. 8a, b). Nevertheless, there are some biases. From Fig. 8c, there is less rainfall in the South Pacific Convergence Zone (SPCZ). Over land, there are 6 mm d^{-1} and 3 mm d^{-1} less rainfall in northern South America and in South Africa, respectively. However, the precipitation is 1–2 mm d^{-1} more over the Tibetan plateau and the west coast of Canada. In boreal summer, the large rainfall is mainly distributed along the equator and the Asian monsoon area. The large precipitation centers over the Bay of Bengal and Philippines are simulated well, and the rainfall over the broad areas from the eastern continents to the oceans in the northern hemisphere is also close to the observation (Fig. 8d, e). Nevertheless, compared to the Xie-Arkin data, biases still exist (Fig. 8f). The rainfall center over the Bay of Bengal extends too far eastward. Near the equator, there is more rainfall over the western Pacific while less over the eastern Pacific. In addition, there is more precipitation of about

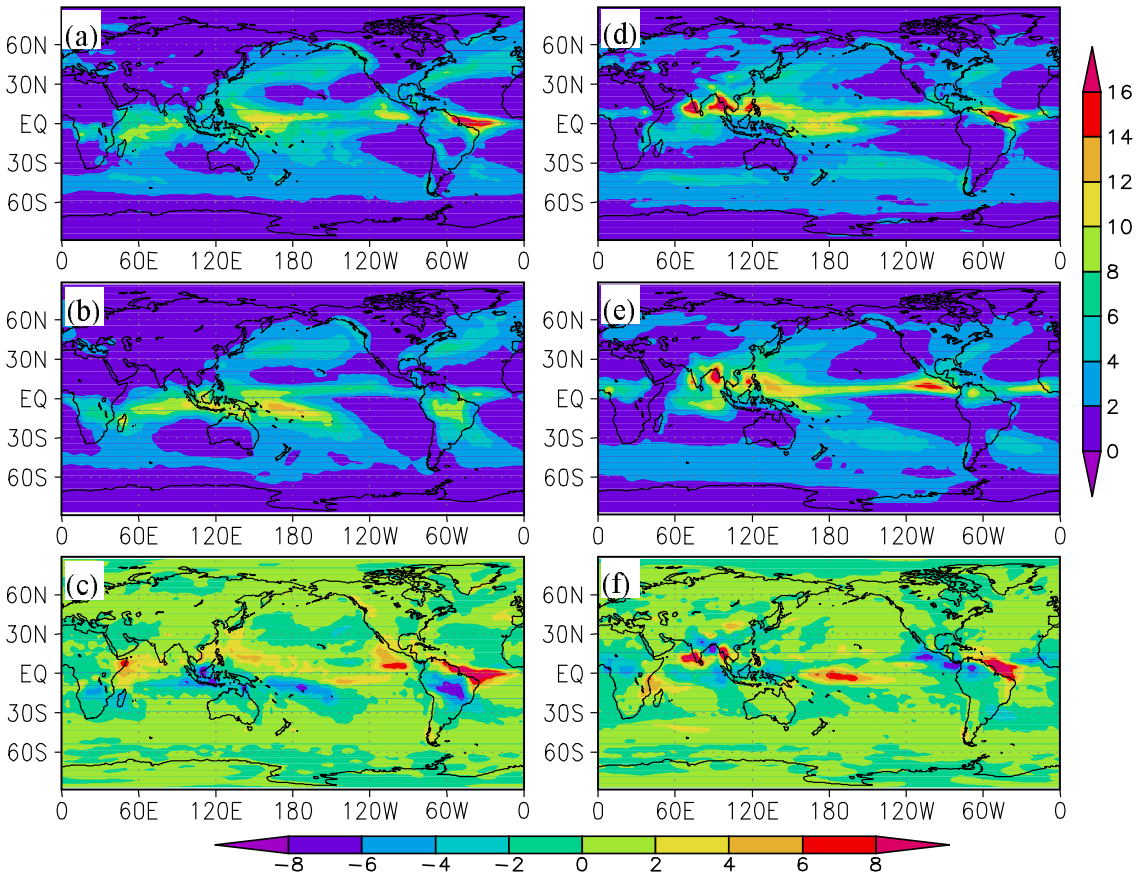

Fig. 8. The (a, b, c) DJF, (d, e, f) JJA mean precipitation rate derived from (a, d) R42_AVIM, (b, e) XIE-ARKIN, and (c, f) the differences between R42_AVIM and XIE-ARKIN, Units: mm d^{-1}.

3–4 mm d^{-1} in northern China. About 4 mm d^{-1} less rainfall exists in tropical Africa and northern South America, while more precipitation is simulated over the southwestern Indian peninsula. The simulated precipitation by R42_SSIB is similar to that of R42_AVIM. However, in DJF, R42_SSIB has much more precipitation in tropical Africa. In JJA, R42_SSIB has much more precipitation on the Tibetan Plateau and about 2 mm d^{-1} less precipitation over the land of Northern Hemisphere.

4.6 *Sea level pressure* (*SLP*)

The simulation of sea level pressure (SLP) can indicate a GCM's ability to simulate the atmospheric circulation near the surface. Figure 9 shows the global distribution of SLP derived from R42_AVIM, NCEP reanalysis and their difference. The basic patterns of SLP in DJF (Fig. 9b) and JJA (Fig. 9e) are well reproduced by R42_AVIM (Figs. 9a, d). In the Northern Hemisphere, the Aleutian Low, Icelandic low and the Mongolia High during DJF, as well as the subtropical high pressure over the Pacific and Atlantic during JJA are all reproduced well by R42_AVIM. For the southern hemisphere, in both seasons, a nearly continuous low-pressure zone close to equator and a belt of subtropical high pressure with centers over the oceans are well simulated (Figs. 9a, d). However, in DJF, the simulated SLP along 40°–70°N is lower (Fig. 9c), indicating that the Mongolia high is weaker and Aleutian and Icelandic lows are stronger than in the NCEP reanalysis. Nevertheless, the simulated SLP over the subtropical areas of Northern Hemisphere and Antarctic has a high bias (Fig. 9c). In boreal summer, there is a high bias of 2–4 hPa over the northern continents except over the Tibetan plateau (Fig. 9f). Lower SLP over the Tibetan Plateau may be attributed to the warm bias of the *in situ* surface air temperature (Fig. 2c). However, over the oceans, the simulated SLP is lower than that in the NCEP reanalysis to a certain extent. The possible reason is that in this work, SST is prescribed as the climate mean so the interaction between atmosphere and sea is missed.

4.7 *Vertical distribution of zonal mean wind*

By analyzing the vertical distribution of the zonal mean wind, we can evaluate the model's ability to sim-

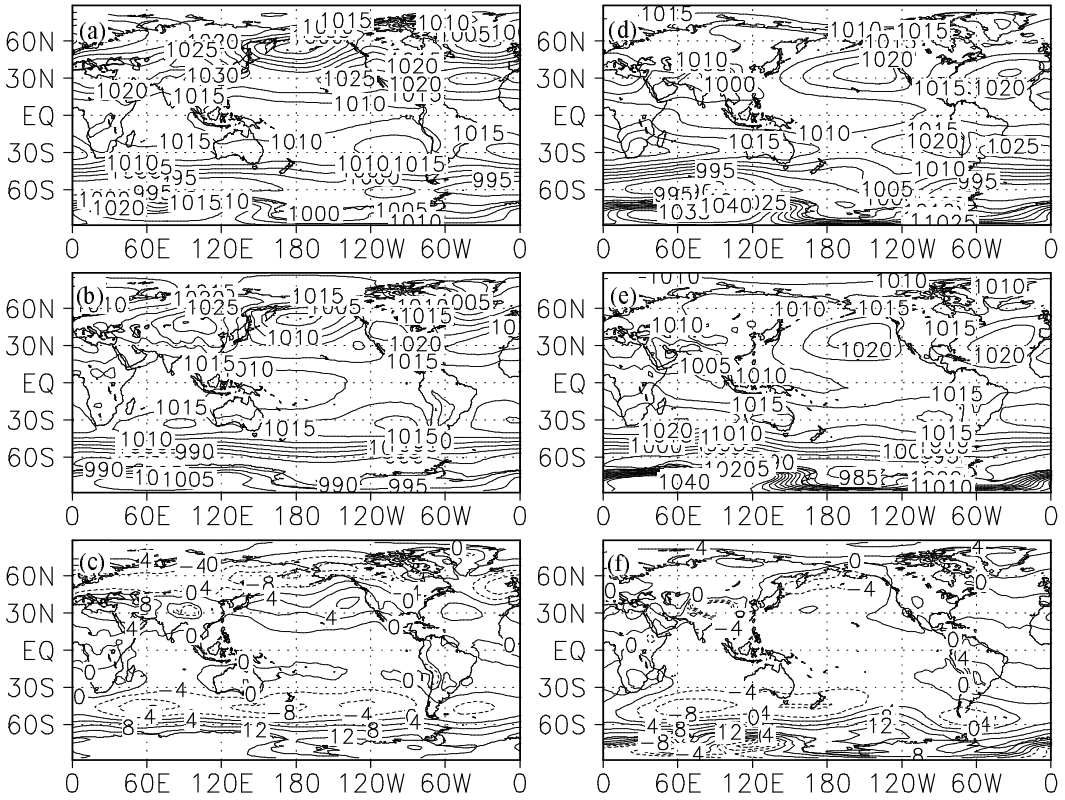

Fig. 9. The DJF, JJA mean sea level pressure derived from (a, d) R42_AVIM, (b, e) NCEP, and (c, f) the differences between R42_AVIM and NCEP, Units: hPa.

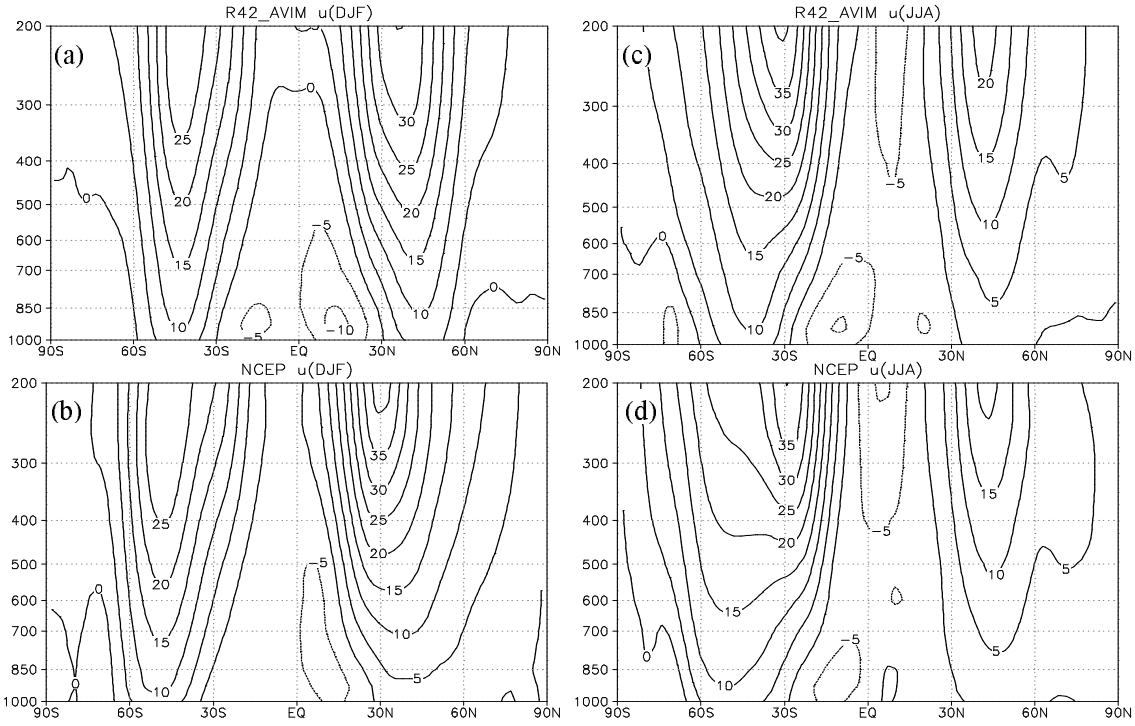

Fig. 10. The DJF, JJA mean zonal wind derived from (a, c) R42_AVIM and (b, d) NCEP. Units: m s^{-1}.

ulate the atmospheric vertical structure. Figure 10 shows the vertical distribution of the mean zonal wind from R42_AVIM and NCEP reanalysis. In winter (Figs. 10a, b), the westerly jet maximum centers in both hemispheres are close to 200 hPa, which is well reproduced by R42_AVIM. However, the intensity of the westerly jet in the northern hemisphere is weaker and extends more northward than in the NCEP reanalysis. In the southern hemisphere, the simulated westerly jet is distributed within narrower latitudes than the observation. In the tropical regions, R42_AVIM simulates the distribution of the easterlies in the low layers well with large wind speed situated in the northern hemisphere. However, the simulated wind speed below 500 hPa is larger than in the NCEP reanalysis. In boreal summer, the simulation of zonal mean wind is quite close to the observation (Figs. 10c, d), although the westerly jets in R42_AVIM are a little stronger in both hemispheres. In the tropical regions, the large wind speed in the low layers is situated in the southern hemisphere, whereas above the middle troposphere, the simulated easterly wind is weaker than that in the NCEP reanalysis.

5. Conclusions

A new two-way land-atmosphere interaction model (R42_AVIM) is fulfilled by coupling of a general circulation model SAMIL_R42L9 with a land surface model AVIM. In this coupled model, physical and physiological components of AVIM are both included. So, LAI is not prescribed but dynamically computed, and the two-way interaction between vegetation and atmosphere is realized.

In this study, the climatic basic state and the surface physical fluxes are analyzed and compared with their counterparts in a one-way coupled model R42_SSIB and in the NCEP reanalysis. The results show that, compared to the one-way coupling, the performance of the new model is much closer to the observations. This model can efficiently guarantee energy balance at the land surface, and can simulate JJA and DJF land surface air temperature, sensible heat flux, latent heat flux, precipitation, sea level pressure etc. reasonably well.

By adding physiological process into the AVIM, the surface parameters such as albedo, vegetation evaporation and transpiration are corrected. Compared to the one-way coupled R42_SSIB (which is coupled by SAMIL_R42L9 and SSIB), obvious improvements in the JJA simulations of surface air temperature and surface fluxes have been obtained. For example, the simulated surface air temperature has an obviously warm bias by R42_SSIB in the broad areas of the Asian and North American continents. This bias is greatly diminished in R42_AVIM. In addition, the simulated sensible and latent heat flux by R42_AVIM is more realistic than R42_SSIB. As a result, the simulations of the atmospheric circulation and the rainfall distribution by R42_AVIM have been improved considerably. It is approved that this land-atmosphere coupled model can offer a good experiment platform for land-atmosphere interaction studies.

Acknowledgements. This study is jointly supported by the National Key Basic Research 2006CB403607, the Chinese Academy of Sciences (CAS) International Partnership Creative Group "The climate system model development and application studies" and the National Natural Science Foundation of China under Grant Nos. 40221503, 40475027 and 40523001.

REFERENCES

Bonan, G., 2002: *Ecological Climatology: Concepts and Applications*. Cambridge University Press, 678pp.

Charney, J. G., 1975: Dynamics of deserts and drought in the Sahel. *Quart. J. Roy. Meteor. Soc.*, **101**(428), 193–202.

Charney, J. G., W. J. Quirk, S. H. Chow, and J. Kornfield, 1977: A comparative study of the effects of albedo change on drought in semiarid regions. *J. Atmos. Sci.*, **34**(9), 1366–1385.

Cox, P. M., 2001: Bringing life and carbon to the GCM land surface processes. *BAHC/GEWEX News Joint Issue*, 10–11.

Dan, L., J. J. Ji, and Y. P. Li, 2005: Climatic and biological simulations in a two-way coupled atmospheric-biosphere model (CABM). *Global and Planetary Change*, **47**, 153–169.

Edwards, J. M., and A. Slingo, 1996: Studies with a flexible new radiation code. I: Choosing a configuration for a large-scale model. *Quart. J. Roy. Meteor. Soc.*, **122**, 689–719.

Foley, J. A., S. Levis, I. C. Prentice, D. Pollard, and S. L. Thompson, 1998: Coupling dynamic models of climate and vegetation. *Global Change Biology*, **4**, 561–579.

Ji, J. J., 1995: A climate-vegetation interaction model: Simulating physical and biological processes at the surface. *Journal of Biogeography*, **22**, 445–451.

Ji, J. J., and Y. C. Hu, 1989: A simple land surface process model for use in climate studies. *Acta Meteorologica Sinica*, **3**, 342–351.

Ji, J. J., and L. Yu, 1999: A simulation study of coupled feedback mechanism between physical and biogeochemical processes at the surface. *Chinese J. Atmos. Sci.*, **23**, 439–448.

Kalnay, E., and Coauthors, 1996: The NCEP/NCAR 40-year reanalysis project. *Bull. Amer. Meteor. Soc.*, **77**, 437–471.

Kaufmann, R. K., R. B. Myneri, C. J. Tucker, D. Slay-

back, N. V. Shabanov, and J. Pinzon, 2003: The effect of vegetation on surface temperature: A statistical analysis of NDVI and climate data. *Geophys. Res. Lett.*, **30**, 2147.

Li, Y. P., and J. J. Ji, 2001: Model estimates of global carbon flux between vegetation and the atmosphere. *Adv. Atmos. Sci.*, **18**, 807–818.

Lu, J. H., 1999: The regional simulation of interaction between atmosphere and vegetation at seasonal and interannual scale. Ph. D dissertation, Institute of Atmospheric Physics, Chinese Academy of Sciences, 160pp. (in Chinese)

Lu, J. H., and J. J. Ji, 2002a: A simulation study of atmosphere-vegetation interactions over the Tibetan Plateau, Part I: Physical fluxes and parameters. *Chinese J. Atmos. Sci.*, **26**, 111–126. (in Chinese)

Lu, J. H., and J. J. Ji, 2002b: A simulation study of atmosphere-vegetation interactions over the Tibetan Plateau, Part II: net primary productivity and leaf index. *Chinese J. Atmos. Sci.*, **26**, 254–262. (in Chinese)

Lu, J. H., and J. J. Ji, 2006: A simulation and mechanism analysis of long-term variations at land surface over arid/semi-arid area in north China. *J. Geophys. Res.*, **111**, D09306, doi: 10.1029/2005JD006252

Lu, L., R. A. Pielke, Sr., G. E. Liston, W. Parton, D. Ojima, and M. Hartman, 2001: Implementation of a two-way interactive atmospheric and ecological model and its application to the Central United States. *J. Climate*, **14**, 900–919.

Manabe, S., J. Smagorinsky, and R. F. Strickler, 1965: Simulated climatology of a general circulation model with a hydrologic cycle. *Mon. Wea. Rev.*, **93**, 769–798.

Pielke, R., R. Avissar, M. Raupach, A. J. Dolman, X. Zhen, and A. S. Denning, 1998: Interactions between the atmosphere and terrestrial ecosystems: Influence on weather and climate. *Global Change Biology*, **4**, 461–475.

Sellers, P. J., 1992: Biophysical models of land surface processes. *Climate System Modeling*, K. E. Trenberth Ed., Cambridge University Press, 451–490.

Shukla, J., and Y. Mintz, 1982: The influence of land-surface evapotranspiration on Earth's climate. *Science*, **215**, 1498–1501.

Simmons, A. J., and J. K. Gibson, 2000: The ERA-40 project plan. *ERA-40 Project Report Series*, No. 1, European Center for Medium-Range Weather Forecasts, Reading, U. K., 31pp.

Slingo, J. M., 1987: The development and verification of a cloud prediction scheme for the ECMWF model. *Quart. J. Roy. Meteor. Soc.*, **113**, 899–927.

Snyder, P. K., J. A. Foley, M. H. Hitchman, and C. Delire, 2004: Analyzing the effects of complete tropical forest removal on the regional climate using a detailed three-dimensional energy budget: A application to Africa. *J. Geophys. Res.*, **109**, D21102, doi: 10.1029/2003JD004462.

Sud, Y. C., and W. E. Smith, 1985: The Influence of land surface roughness of deserts on the July circulation-A numerical study. *Bound.-Layer Meteor.*, **33**(1), 15–49.

Tsvetsinskaya, E. A., L. O. Mearns, and W. E. Easterling, 2001: Investigating the effect of seasonal plant growth and development in 3-dimensional atmospheric simulations: Part I. Simulations of Surface Fluxes over the Growing Season. *J. Climate*, **14**, 692–709.

Uppala, S. M., and Coauthors, 2005: The ERA-40 reanalysis. *Quart. J. Roy. Meteor. Soc.*, **131**, 2961–3012. doi: 10.1256/qj.04.176

Wang, Z. Z., G. X. Wu, T. W. Wu, and R. C. Yu, 2004: Simulation of Asia monsoon seasonal variations with climate model R42L9/LASG. *Adv. Atmos. Sci.*, **21**, 879–889.

Wu, T. W., P. Liu, Z. Z. Wang, Y. M. Liu, R. C. Yu, and G. X. Wu, 2003: The performance of Atmospheric Component Model R42L9 of GOALS/LASG. *Adv. Atmos. Sci.*, **20**, 726–742.

Xie, P., and P. A. Arkin, 1996: Analyses of global monthly precipitation using gauge observations, satellite estimates, and numerical model predictions. *J. Climate*, **9**, 840–858.

Yeh, T. C., R. I. Wetherald, and S. Manabe, 1984: The effects of soil moisture on the short-term climate and hydrology change—A numerical experiment. *Mon. Wea. Rev.*, **112**, 474–490.

Zhang, X. H., G. Y. Shi, H. Liu, and Y. Q. Yu, 2000: *IAP Global Ocean-Atmosphere-Land System Model*, Science Press, Beijing, 252pp.

Zeng, Q. C., 1963: Characteristic parameter and dynamical equation of atmospheric motions. *Acta Meteoroogica Sinica*, **33**, 472–483. (in Chinese)